Observation of χ_{cJ} decaying into the $p\bar{p}K^+K^-$ final state

M. Ablikim,[1] M. N. Achasov,[5] D. Alberto,[38] L. An,[9] Q. An,[36] Z. H. An,[1] J. Z. Bai,[1] R. Baldini,[17] Y. Ban,[23] J. Becker,[2] N. Berger,[1] M. Bertani,[17] J. M. Bian,[1] O. Bondarenko,[16] I. Boyko,[15] R. A. Briere,[3] V. Bytev,[15] X. Cai,[1] G. F. Cao,[1] X. X. Cao,[1] J. F. Chang,[1] G. Chelkov,[15,*] G. Chen,[1] H. S. Chen,[1] J. C. Chen,[1] M. L. Chen,[1] S. J. Chen,[1] Y. Chen,[1] Y. B. Chen,[1] H. P. Cheng,[11] Y. P. Chu,[1] D. Cronin-Hennessy,[35] H. L. Dai,[1] J. P. Dai,[1] D. Dedovich,[15] Z. Y. Deng,[1] I. Denysenko,[15,†] M. Destefanis,[38] Y. Ding,[19] L. Y. Dong,[1] M. Y. Dong,[1] S. X. Du,[42] R. R. Fan,[1] J. Fang,[1] S. S. Fang,[1] C. Q. Feng,[36] C. D. Fu,[1] J. L. Fu,[21] Y. Gao,[32] C. Geng,[36] K. Goetzen,[7] W. X. Gong,[1] M. Greco,[38] S. Grishin,[15] M. H. Gu,[1] Y. T. Gu,[9] Y. H. Guan,[6] A. Q. Guo,[22] L. B. Guo,[20] Y. P. Guo,[22] X. Q. Hao,[1] F. A. Harris,[34] K. L. He,[1] M. He,[1] Z. Y. He,[22] Y. K. Heng,[1] Z. L. Hou,[1] H. M. Hu,[1] J. F. Hu,[6] T. Hu,[1] B. Huang,[1] G. M. Huang,[12] J. S. Huang,[10] X. T. Huang,[25] Y. P. Huang,[1] T. Hussain,[37] C. S. Ji,[36] Q. Ji,[1] X. B. Ji,[1] X. L. Ji,[1] L. K. Jia,[1] L. L. Jiang,[1] X. S. Jiang,[1] J. B. Jiao,[25] Z. Jiao,[11] D. P. Jin,[1] S. Jin,[1] F. F. Jing,[32] N. Kalantar-Nayestanaki,[16] M. Kavatsyuk,[16] S. Komamiya,[31] W. Kuehn,[33] J. S. Lange,[33] J. K. C. Leung,[30] Cheng Li,[36] Cui Li,[36] D. M. Li,[42] F. Li,[1] G. Li,[1] H. B. Li,[1] J. C. Li,[1] Lei Li,[1] N. B. Li,[20] Q. J. Li,[1] W. D. Li,[1] W. G. Li,[1] X. L. Li,[25] X. N. Li,[1] X. Q. Li,[22] X. R. Li,[1] Z. B. Li,[28] H. Liang,[36] Y. F. Liang,[27] Y. T. Liang,[33] G. R. Liao,[8] X. T. Liao,[1] B. J. Liu,[29] B. J. Liu,[30] C. L. Liu,[3] C. X. Liu,[1] C. Y. Liu,[1] F. H. Liu,[26] Fang Liu,[1] Feng Liu,[12] G. C. Liu,[1] H. Liu,[1] H. B. Liu,[6] H. M. Liu,[1] H. W. Liu,[1] J. P. Liu,[1] K. Liu,[40] K. Y. Liu,[19] Q. Liu,[34] S. B. Liu,[36] X. Liu,[18] X. H. Liu,[1] Y. B. Liu,[22] Y. W. Liu,[36] Yong Liu,[1] Z. A. Liu,[1] Z. Q. Liu,[1] H. Loehner,[16] G. R. Lu,[10] H. J. Lu,[11] J. G. Lu,[1] Q. W. Lu,[26] X. R. Lu,[6] Y. P. Lu,[1] C. L. Luo,[20] M. X. Luo,[41] T. Luo,[1] X. L. Luo,[1] C. L. Ma,[6] F. C. Ma,[19] H. L. Ma,[1] Q. M. Ma,[1] T. Ma,[1] X. Ma,[1] X. Y. Ma,[1] M. Maggiora,[38] Q. A. Malik,[37] H. Mao,[1] Y. J. Mao,[23] Z. P. Mao,[1] J. G. Messchendorp,[16] J. Min,[1] R. E. Mitchell,[14] X. H. Mo,[1] N. Yu. Muchnoi,[5] Y. Nefedov,[15] Z. Ning,[1] S. L. Olsen,[24] Q. Ouyang,[1] S. Pacetti,[17] M. Pelizaeus,[34] K. Peters,[7] J. L. Ping,[20] R. G. Ping,[1] R. Poling,[35] C. S. J. Pun,[30] M. Qi,[21] S. Qian,[1] C. F. Qiao,[6] X. S. Qin,[1] J. F. Qiu,[1] K. H. Rashid,[37] G. Rong,[1] X. D. Ruan,[9] A. Sarantsev,[15,‡] J. Schulze,[2] M. Shao,[36] C. P. Shen,[34] X. Y. Shen,[1] H. Y. Sheng,[1] M. R. Shepherd,[14] X. Y. Song,[1] S. Sonoda,[31] S. Spataro,[38] B. Spruck,[33] D. H. Sun,[1] G. X. Sun,[1] J. F. Sun,[10] S. S. Sun,[1] X. D. Sun,[1] Y. J. Sun,[36] Y. Z. Sun,[1] Z. J. Sun,[1] Z. T. Sun,[36] C. J. Tang,[27] X. Tang,[1] X. F. Tang,[8] H. L. Tian,[1] D. Toth,[35] G. S. Varner,[34] X. Wan,[1] B. Q. Wang,[23] K. Wang,[1] L. L. Wang,[4] L. S. Wang,[1] M. Wang,[25] P. Wang,[1] P. L. Wang,[1] Q. Wang,[1] S. G. Wang,[23] X. L. Wang,[36] Y. D. Wang,[36] Y. F. Wang,[1] Y. Q. Wang,[25] Z. Wang,[1] Z. G. Wang,[1] Z. Y. Wang,[1] D. H. Wei,[8] Q. G. Wen,[36] S. P. Wen,[1] U. Wiedner,[2] L. H. Wu,[1] N. Wu,[1] W. Wu,[19] Z. Wu,[1] Z. J. Xiao,[20] Y. G. Xie,[1] G. F. Xu,[1] G. M. Xu,[23] H. Xu,[1] Y. Xu,[22] Z. R. Xu,[36] Z. Z. Xu,[36] Z. Xue,[1] L. Yan,[36] W. B. Yan,[36] Y. H. Yan,[13] H. X. Yang,[1] M. Yang,[1] T. Yang,[9] Y. Yang,[12] Y. X. Yang,[8] M. Ye,[1] M. H. Ye,[4] B. X. Yu,[1] C. X. Yu,[22] L. Yu,[12] C. Z. Yuan,[1] W. L. Yuan,[20] Y. Yuan,[1] A. A. Zafar,[37] A. Zallo,[17] Y. Zeng,[13] B. X. Zhang,[1] B. Y. Zhang,[1] C. C. Zhang,[1] D. H. Zhang,[1] H. H. Zhang,[28] H. Y. Zhang,[1] J. Zhang,[20] J. W. Zhang,[1] J. Y. Zhang,[1] J. Z. Zhang,[1] L. Zhang,[21] S. H. Zhang,[1] T. R. Zhang,[20] X. J. Zhang,[1] X. Y. Zhang,[25] Y. Zhang,[1] Y. H. Zhang,[1] Z. P. Zhang,[36] Z. Y. Zhang,[40] G. Zhao,[1] H. S. Zhao,[1] Jiawei Zhao,[36] Jingwei Zhao,[1] Lei Zhao,[36] Ling Zhao,[1] M. G. Zhao,[22] Q. Zhao,[1] S. J. Zhao,[42] T. C. Zhao,[39] X. H. Zhao,[21] Y. B. Zhao,[1] Z. G. Zhao,[36] Z. L. Zhao,[9] A. Zhemchugov,[15,*] B. Zheng,[1] J. P. Zheng,[1] Y. H. Zheng,[6] Z. P. Zheng,[1] B. Zhong,[1] J. Zhong,[2] L. Zhong,[32] L. Zhou,[1] X. K. Zhou,[6] X. R. Zhou,[36] C. Zhu,[1] K. Zhu,[1] K. J. Zhu,[1] S. H. Zhu,[1] X. L. Zhu,[32] X. W. Zhu,[1] Y. S. Zhu,[1] Z. A. Zhu,[1] J. Zhuang,[1] B. S. Zou,[1] J. H. Zou,[1] J. X. Zuo,[1] and P. Zweber[35]

(BESIII Collaboration)

[1]*Institute of High Energy Physics, Beijing 100049, P. R. China*
[2]*Bochum Ruhr-University, 44780 Bochum, Germany*
[3]*Carnegie Mellon University, Pittsburgh, Pennsylvania 15213, USA*
[4]*China Center of Advanced Science Technology, Beijing 100190, P. R. China*
[5]*G. I. Budker Institute of Nuclear Physics SB RAS (BINP), Novosibirsk 630090, Russia*
[6]*Graduate University of Chinese Academy of Sciences, Beijing 100049, P. R. China*
[7]*GSI Helmholtzcentre for Heavy Ion Research GmbH, D-64291 Darmstadt, Germany*
[8]*Guangxi Normal University, Guilin 541004, P. R. China*
[9]*Guangxi University, Naning 530004, P. R. China*
[10]*Henan Normal University, Xinxiang 453007, P. R. China*
[11]*Huangshan College, Huangshan 245000, P. R. China*
[12]*Huazhong Normal University, Wuhan 430079, P. R. China*
[13]*Hunan University, Changsha 410082, P. R. China*
[14]*Indiana University, Bloomington, Indiana 47405, USA*
[15]*Joint Institute for Nuclear Research, 141980 Dubna, Russia*

[16]*KVI/University of Groningen, 9747 AA Groningen, The Netherlands*
[17]*Laboratori Nazionali di Frascati-INFN, 00044 Frascati, Italy*
[18]*Lanzhou University, Lanzhou 730000, P. R. China*
[19]*Liaoning University, Shenyang 110036, P. R. China*
[20]*Nanjing Normal University, Nanjing 210046, P. R. China*
[21]*Nanjing University, Nanjing 210093, P. R. China*
[22]*Nankai University, Tianjin 300071, P. R. China*
[23]*Peking University, Beijing 100871, P. R. China*
[24]*Seoul National University, Seoul, 151-747 Korea*
[25]*Shandong University, Jinan 250100, P. R. China*
[26]*Shanxi University, Taiyuan 030006, P. R. China*
[27]*Sichuan University, Chengdu 610064, P. R. China*
[28]*Sun Yat-Sen University, Guangzhou 510275, P. R. China*
[29]*The Chinese University of Hong Kong, Shatin, N.T., Hong Kong*
[30]*The University of Hong Kong, Pokfulam Hong Kong*
[31]*The University of Tokyo, Tokyo 113-0033 Japan*
[32]*Tsinghua University, Beijing 100084, P. R. China*
[33]*Universitaet Giessen, 35392 Giessen, Germany*
[34]*University of Hawaii, Honolulu, Hawaii 96822, USA*
[35]*University of Minnesota, Minneapolis, Minnesota 55455, USA*
[36]*University of Science and Technology of China, Hefei 230026, P. R. China*
[37]*University of the Punjab, Lahore-54590, Pakistan*
[38]*University of Turin and INFN, Turin, Italy*
[39]*University of Washington, Seattle, Washington 98195, USA*
[40]*Wuhan University, Wuhan 430072, P. R. China*
[41]*Zhejiang University, Hangzhou 310027 P. R. China*
[42]*Zhengzhou University, Zhengzhou 450001, P. R. China*
(Received 15 March 2011; published 27 June 2011)

First measurements of the decays of the three χ_{cJ} states to $p\bar{p}K^+K^-$ final states are presented. Intermediate $\phi \to K^+K^-$ and $\Lambda(1520) \to pK^-$ resonance states are observed, and branching fractions for $\chi_{cJ} \to \bar{p}K^+\Lambda(1520)$, $\Lambda(1520)\bar{\Lambda}(1520)$, and $\phi p\bar{p}$ are reported. We also measure branching fractions for direct $\chi_{cJ} \to p\bar{p}K^+K^-$ decays. These are first observations of χ_{cJ} decays to unstable baryon resonances and provide useful information about the χ_{cJ} states. The experiment uses samples of χ_{cJ} mesons produced via radiative transitions from 106×10^6 ψ' mesons collected in the BESIII detector at the BEPCII e^+e^- collider.

DOI: 10.1103/PhysRevD.83.112009 PACS numbers: 13.25.Gv, 14.20.Pt, 14.40.Be

I. INTRODUCTION

Experimental studies on charmonia decay properties are useful for testing perturbative QCD models and QCD-based calculations. In the standard quark model, the $\chi_{cJ}(J = 0, 1, 2)$ mesons are P-wave quarkonium states with spin parity 0^{++}, 1^{++}, and 2^{++}. Although they cannot be produced directly in e^+e^- collisions, radiative decays of the ψ' into each χ_{cJ} occur about 9% [1] of the time and provide large χ_{cJ} samples that have proven to be a very clean environment for studies of the χ_{cJ} states.

The color octet mechanism (COM) has been shown to play an important role in describing these P-wave quarkonium decays [2–5]. Many COM predictions for χ_{cJ} decays into meson pairs and $p\bar{p}$ pairs are in agreement with earlier experimental results. However, the predictions for some baryon-antibaryon decays disagree with measured values, in particular $\chi_{cJ} \to \Lambda\bar{\Lambda}$ [6]. At present, only ground state baryons have been observed in χ_{cJ} decays [1]. To further test COM predictions for P-wave charmonia decay, measurements of excited baryon pair decays are important. This paper presents a study of χ_{cJ} hadronic decays and measurements of $\chi_{cJ} \to \Lambda(1520)\bar{\Lambda}(1520)$ decaying to $p\bar{p}K^+K^-$, based on 106×10^6 ψ' events collected with BESIII at BEPCII. The observation of such excited baryon production can provide constraints on models of P-wave charmonia hadronic decay.

II. DETECTOR

BEPCII [7] is a double-ring e^+e^- collider designed to provide a peak luminosity of 10^{33} cm^{-2} s^{-1} at the center of mass energy of 3770 MeV. The BESIII [7] detector has a geometrical acceptance of 93% of 4π and has four main

[*]also at the Moscow Institute of Physics Technology, Moscow Russia.
[†]on leave from the Bogolyubov Institute for Theoretical Physics, Kiev, Ukraine.
[‡]also at the PNPI, Gatchina, Russia.

components: (1) A small-cell, helium-based (40% He, 60% C_3H_8) main drift chamber (MDC) with 43 layers providing an average single-hit resolution of 135 μm, and charged-particle momentum resolution in a 1 T magnetic field of 0.5% at 1 GeV/c. (2) An electromagnetic calorimeter (EMC) consisting of 6240 CsI(Tl) crystals in a cylindrical structure (barrel) and two endcaps. The energy resolution at 1.0 GeV/c is 2.5% (5%) in the barrel (endcaps), and the position resolution is 6 mm (9 mm) in the barrel (endcaps). (3) Particle identification is provided by a time-of-flight system constructed of 5 cm-thick plastic scintillators, with 176 detectors of 2.4 m length in two layers in the barrel and 96 fan-shaped detectors in the endcaps. The barrel (endcap) time resolution of 80 ps (110 ps) provides 2σ K/π separation for momenta up to $\sim$1.0 GeV/c. (4) The muon system consists of 1000 m^2 of resistive plate chambers in nine barrel and eight endcap layers and provides 2 cm position resolution.

III. MONTE-CARLO SIMULATION

Monte-Carlo (MC) simulation of the full detector is used to determine the detection efficiency of each channel, optimize event selection criteria, and estimate backgrounds. The simulation program, BOOST, provides an event generator, contains the detector geometry description, and simulates the detector response and signal digitization. Charmonium resonances, such as the ψ', are generated by KKMC [8,9], which accounts for effects such as initial state radiation and beam energy spread. The subsequent charmonium meson decays are produced with BesEvtGen [10,11]. The detector geometry and material description and the tracking of the decay particles through the detector including interactions are handled by Geant4.

IV. EVENT SELECTION

Charged tracks must have their point of closest approach to the beamline within $\pm$10 cm of the interaction point in the beam direction and within 1 cm of the beamline in the plane perpendicular to the beam and must have the polar angle satisfy $|\cos\theta| < 0.93$. The time-of-flight and energy loss dE/dx measurements are combined to calculate particle identification (PID) probabilities for pion, kaon, and proton/antiproton hypotheses, and each track is assigned a particle type corresponding to the hypothesis with the highest confidence level (C.L.). Finally, four tracks identified as p, $\bar{p}$ K^+, and K^- are required.

Photon candidates are selected by requiring a minimum energy deposition of 80 MeV in the EMC. EMC cluster timing requirements suppress electronic noise and energy deposits unrelated to the event.

Kinematic fitting that utilizes momentum and energy conservation is applied under the hypothesis $\psi' \to \gamma\chi_{cJ} \to \gamma p\bar{p}K^+K^-$. For events with more than one photon candidate, the combination with the smallest χ^2_{4C} is considered for further analysis.

V. DATA ANALYSIS

After candidate event selection, distinct χ_{cJ} signals are observed in the $p\bar{p}K^+K^-$ invariant mass distribution, as shown in Fig. 1(a). By combining final state particles (p, $\bar{p}$, K^+, K^-), the $\Lambda(1520)$, $\bar{\Lambda}(1520)$, and ϕ intermediate states can also be seen in the pK^-, $\bar{p}K^+$, and K^+K^- invariant mass distributions, as shown in Fig. 1(b)–1(d), respectively.

A. Background studies

A sample of 100×10^6 inclusive ψ' MC events is used to investigate possible backgrounds. No background events survive after candidate selection.

Potential physics background contributions due to undetected or fake photons and particle misidentification can come from the processes: $\psi' \to \pi^0 p\bar{p}K^+K^-$, $\psi' \to \gamma\chi_{cJ} \to \gamma K^+K^-K^+K^-$, $\gamma K^+K^-\pi^+\pi^-$, $\gamma p\bar{p}\pi^+\pi^-$, and $\psi' \to p\bar{p}K^+K^-$. We produced 2×10^5 MC events for the first process and 1×10^5 MC events for each of the other processes in order to study these backgrounds. After applying the event selection criteria to MC events, 265 events survive, and all of them are from $\psi' \to \pi^0 p\bar{p}K^+K^-$. Since the branching fraction of this channel has not been reported by the PDG [1], we determine it from our data sample and use the result to estimate the background contribution to be about 1.4 events. In addition, a 42.9 pb^{-1} data sample collected at 3.65 GeV is used to investigate possible continuum backgrounds, and no events survive candidate selection.

B. $\chi_{cJ} \to p\bar{p}K^+K^-$

The branching fractions for $\chi_{cJ} \to p\bar{p}K^+K^-$ are measured excluding the evident $\Lambda(1520)$, $\bar{\Lambda}(1520)$, and ϕ intermediate states seen in Fig. 1(b)–1(d), by vetoing these events with the mass requirements $|M(pK^-) - 1.52| > 0.07$ GeV/c^2, $|M(\bar{p}K^+) - 1.52| > 0.07$ GeV/c^2, and $|M(K^+K^-) - 1.02| > 0.03$ GeV/c^2. The fit of the invariant mass distribution of the remaining candidate events is shown in Fig. 2.

The $p\bar{p}K^+K^-$ mass distribution is fitted with Breit-Wigner functions convolved with Gaussian resolution functions to describe the χ_{cJ} signals and a flat distribution for the background, as shown in Fig. 2. The Breit-Wigner parameters and Gaussian instrumental resolutions are floated in the fit, with the χ_{cJ} widths fixed according to PDG [1] values. The instrumental resolutions are found to be about 4 MeV/c^2, and the masses of the χ_{cJ} from the fit are consistent with PDG values within 1σ. The observed numbers of events, denoted as $N_{\rm obs}$, for $\chi_{cJ} \to p\bar{p}K^+K^-$ decays are listed in Table I. The branching fractions are calculated according to

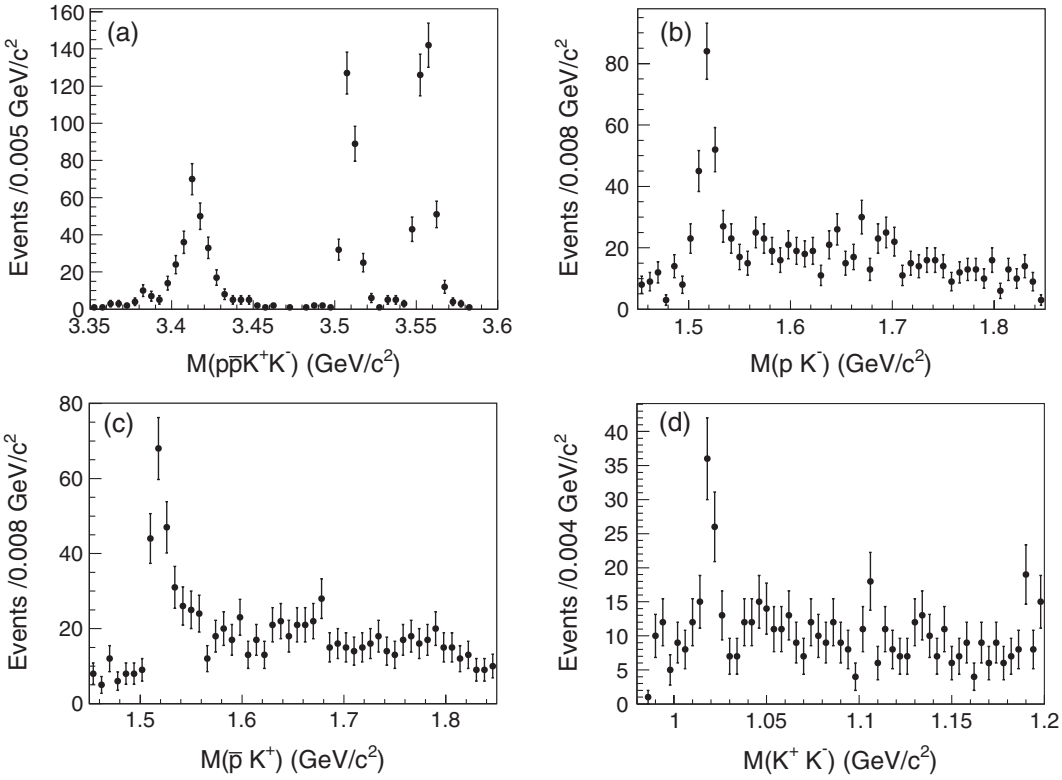

FIG. 1. Invariant mass distributions of (a) $p\bar{p}K^+K^-$, (b) pK^-, (c) $\bar{p}K^+$, and (d) K^+K^-.

$$\mathcal{B}(\chi_{cJ} \to p\bar{p}K^+K^-) = \frac{N_{\rm obs}}{N_{\psi'} \cdot \mathcal{B}(\psi' \to \gamma\chi_{cJ}) \cdot \varepsilon},$$

where $N_{\psi'}$ is the total number of ψ' events, which is measured to be 106×10^6 with an uncertainty of 4% [12], the $\psi' \to \gamma\chi_{cJ}$ branching fractions are taken from PDG [1] to be $(9.62 \pm 0.31)\%$, $(9.2 \pm 0.4)\%$ and $(8.74 \pm 0.35)\%$ for χ_{c0}, χ_{c1} and χ_{c2}, respectively, and the detection efficiencies, ε, are determined individually for simulated

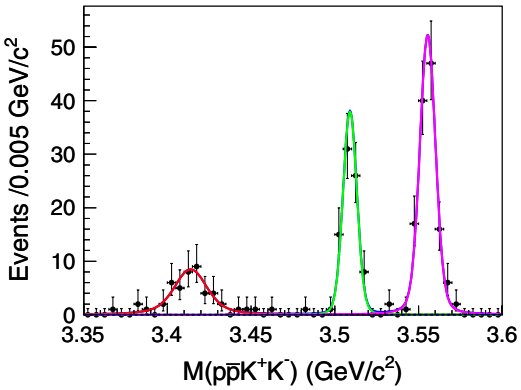

FIG. 2 (color online). The $p\bar{p}K^+K^-$ invariant mass distribution and fit result after excluding $\Lambda(1520)$, $\bar{\Lambda}(1520)$, and ϕ intermediate states, where dots with error bars are data and the solid curves show the fit result. The dashed line, barely perceptible, is the estimated background component.

ψ' decays to $p\bar{p}K^+K^-$ via the χ_{c0}, χ_{c1}, and χ_{c2} states. The results are summarized in Table I.

C. $\chi_{cJ} \to \bar{p}K^+\Lambda(1520)$ + charge conjugate

For analysis of the intermediate states described below, the following invariant mass selection criteria are imposed:

$$\chi_{c0}\text{: } 3.365\ \text{GeV}/c^2 < M(p\bar{p}K^+K^-) < 3.455\ \text{GeV}/c^2,$$
$$\chi_{c1}\text{: } 3.490\ \text{GeV}/c^2 < M(p\bar{p}K^+K^-) < 3.530\ \text{GeV}/c^2,$$
$$\chi_{c2}\text{: } 3.530\ \text{GeV}/c^2 < M(p\bar{p}K^+K^-) < 3.580\ \text{GeV}/c^2.$$

The three-body decay branching fractions $\chi_{cJ} \to \bar{p}K^+\Lambda(1520)$ + c.c. are measured after rejecting the $\bar{\Lambda}(1520)$ for $\bar{p}K^+\Lambda(1520)$ with the requirement $|M(\bar{p}K^+) - 1.52| > 0.07\ \text{GeV}/c^2$ or for the charge conjugate (c.c.) $\Lambda(1520)$ to $pK^-\bar{\Lambda}(1520)$ by $|M(pK^-) - 1.52| > 0.07\ \text{GeV}/c^2$. The fitted pK^- + c.c. invariant

TABLE I. The branching fractions for $\chi_{cJ} \to p\bar{p}K^+K^-$, where errors are statistical only.

Quantity	χ_{c0}	χ_{c1}	χ_{c2}
$N_{\rm obs}$	48.2 ± 7.7	81.5 ± 9.2	131 ± 12
$\varepsilon(\%)$	3.8 ± 0.1	6.2 ± 0.1	6.8 ± 0.1
$\mathcal{B}(\chi_{cJ} \to p\bar{p}K^+K^-)$ (10^{-4})	1.24 ± 0.20	1.35 ± 0.15	2.08 ± 0.19

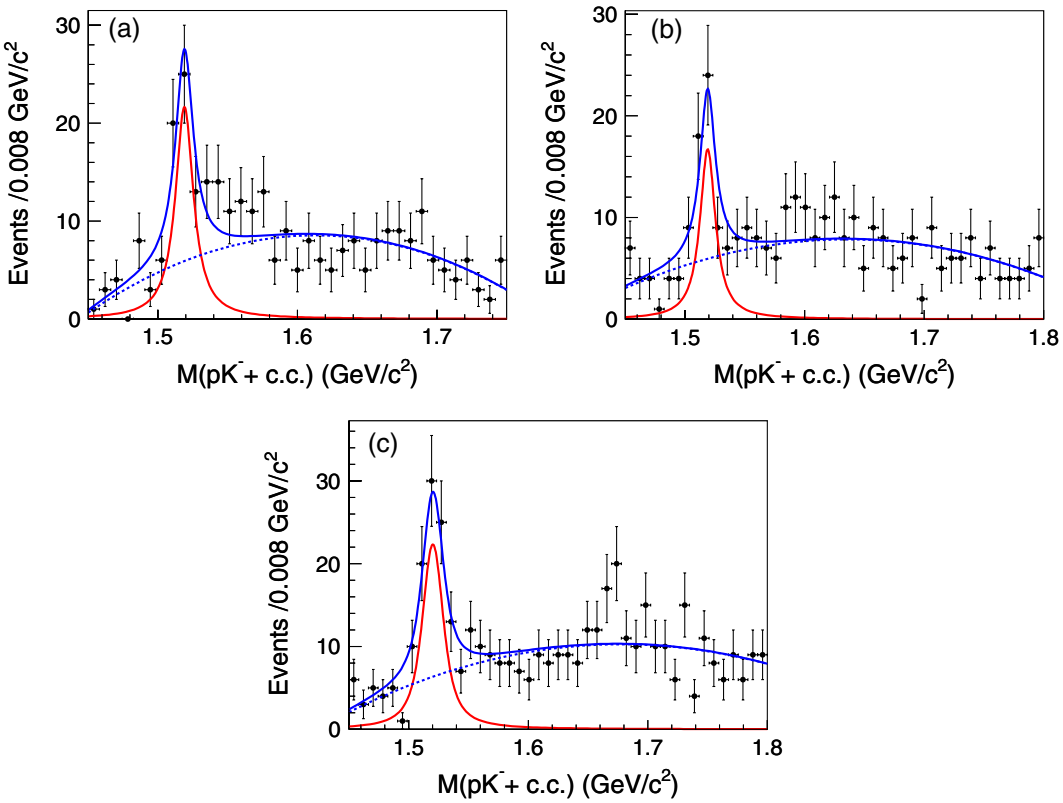

FIG. 3 (color online). Invariant mass distributions and fits to pK^- + c.c. in the decays of (a) χ_{c0}, (b) χ_{c1}, and (c) χ_{c2}. Dots with error bars are data. Solid lines are results of the fit, and dashed curves represent the background.

mass distributions are shown in Fig. 3. The fits use Breit-Wigner functions convolved with Gaussians for the signals and Chebyshev polynomials for backgrounds, where the Breit-Wigner masses and Gaussian instrumental resolution are free parameters, and the widths of the resonances are fixed to their PDG [1] values. The observed numbers of events, $N_{\rm obs}$, for $\chi_{cJ} \to \bar{p}K^+\Lambda(1520)$ + c.c. are shown in Table II.

The branching fractions are calculated according to:

$$\mathcal{B}(\chi_{cJ} \to \bar{p}K^+\Lambda(1520) + \text{c.c.}) = \frac{N_{\rm obs}}{N_{\psi'} \cdot \mathcal{B}(\psi' \to \gamma\chi_{cJ}) \cdot \mathcal{B}(\Lambda(1520) \to pK^-) \cdot \varepsilon},$$

where the detection efficiencies ε are determined by the MC simulation of ψ' decays to $\bar{p}K^+\Lambda(1520)$ + c.c. for each of the χ_{c0}, χ_{c1}, and χ_{c2} states. The results are summarized in Table II.

D. $\chi_{cJ} \to \Lambda(1520)\bar{\Lambda}(1520)$

A scatter plot of the invariant mass $M(\bar{p}K^+)$ versus $M(pK^-)$ is shown in Fig. 4(a), where a signal for $\chi_{cJ} \to \Lambda(1520)\bar{\Lambda}(1520)$ is evident. Events remaining after rejecting $\phi p\bar{p}$ events with the veto requirement $|M(K^+K^-) - 1.02| > 0.03$ GeV/c^2 and satisfying $|M(\bar{p}K^+) - 1.520| < 0.05$ GeV/c^2 and $|M(pK^-) - 1.520| < 0.05$ GeV/c^2 are selected as candidate $\Lambda(1520)\bar{\Lambda}(1520)$ events. Two-dimensional mass sideband regions used to estimate background in the signal region S are indicated by the regions A, B, and C in Fig. 4(a). The events in these sideband regions for data are scaled by factors that are determined by the ratios of events in the signal region S to those in the sideband regions for MC samples for the background

TABLE II. The branching fractions for $\chi_{cJ} \to \bar{p}K^+\Lambda(1520)$ + c.c., where errors are statistical only.

Quantity	χ_{c0}	χ_{c1}	χ_{c2}
$N_{\rm obs}$	62 ± 12	48 ± 10	79 ± 13
ε(%)	9.0 ± 0.1	12.1 ± 0.1	12.4 ± 0.1
$\mathcal{B}(\Lambda(1520) \to pK^-)$(%)	22.5	22.5	22.5
$\mathcal{B}(\chi_{cJ} \to \bar{p}K^+\Lambda(1520) + \text{c.c.})$ (10^{-4})	3.00 ± 0.58	1.81 ± 0.38	3.06 ± 0.50

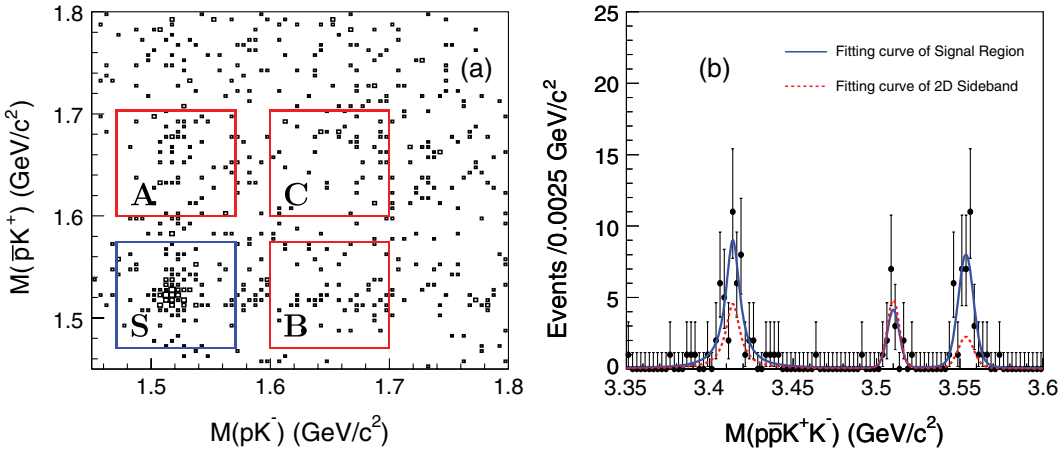

FIG. 4 (color online). (a) Scatter plot of $M(\bar{p}K^+)$ versus $M(pK^-)$; (b) Invariant mass spectrum and fits to $p\bar{p}K^+K^-$, where dots with error bars are events from the signal region. The solid line is the fitting curve for the events from signal region, and the dashed lines represent background estimated from the two-dimensional mass sidebands of regions "A, B, C" as shown in (a).

channels, namely, $\psi' \to \gamma\chi_{cJ} \to \gamma\bar{p}K^+\Lambda(1520)$, $\psi' \to \gamma\chi_{cJ} \to \gamma pK^-\bar{\Lambda}(1520)$, and $\psi' \to \gamma\chi_{cJ} \to \gamma p\bar{p}K^+K^-$, are to estimate the background in the signal region S of the data.

The mass spectra obtained from the signal and scaled sideband background events in Fig. 4(a) are simultaneously fit using Breit-Wigner functions convolved with Gaussian resolution functions. The Breit-Wigner masses and the instrumental resolutions used for the Gaussians are left as free parameters in the fit. Other background is described by a flat distribution. The differences between the results of the fits to the signal and scaled sideband events, shown in Fig. 4(b), are used to extract the $\chi_{cJ} \to \Lambda(1520)\bar{\Lambda}(1520)$ yield. We find 28.1 ± 9.8 events for $\chi_{c0} \to \Lambda(1520)\bar{\Lambda}(1520)$ and 28.9 ± 7.4 events for $\chi_{c2} \to \Lambda(1520)\bar{\Lambda}(1520)$. No distinct $\chi_{c1} \to \Lambda(1520)\bar{\Lambda}(1520)$ signal is observed, and a 90% C.L. upper limit is given using the Bayesian method.

The branching fractions are calculated according to:

$$\mathcal{B}(\chi_{cJ} \to \Lambda(1520)\bar{\Lambda}(1520)) = \frac{N_{\rm obs}}{N_{\psi'} \cdot \mathcal{B}(\psi' \to \gamma\chi_{cJ}) \cdot \mathcal{B}(\Lambda(1520) \to pK^-) \cdot \mathcal{B}(\bar{\Lambda}(1520) \to \bar{p}K^+) \cdot \varepsilon},$$

and the upper limit at the 90% C.L. is calculated as

$$\mathcal{B}(\chi_{c1} \to \Lambda(1520)\bar{\Lambda}(1520)) < \frac{N_{\rm obs}}{N_{\psi'} \cdot \mathcal{B}(\psi' \to \gamma\chi_{c1}) \cdot \mathcal{B}(\Lambda(1520) \to pK^-) \cdot \mathcal{B}(\bar{\Lambda}(1520) \to \bar{p}K^+) \cdot \varepsilon \cdot (1 - \sigma_{\rm sys})},$$

where the detection efficiencies are determined from MC simulation, which assumes an angular distribution of $1 + \alpha\cos^2\theta$ for the two-body decays, and the value for α is estimated by fitting the $\cos\theta$ distribution of data separately for the χ_{c0}, χ_{c1}, and χ_{c2} states, θ is the polar angle of a particle in the rest frame of its mother particle, and $\sigma_{\rm sys}$ denotes the systematic error (discussed below). The results are summarized in Table III.

E. $\chi_{cJ} \to p\bar{p}\phi$

The K^+K^- invariant mass distributions and fits to the spectra are presented in Fig. 5 for the χ_{c0}, χ_{c1}, and χ_{c2}. ϕ signals are observed clearly in the decays of χ_{c0} [Fig. 5(a)] and χ_{c2} [Fig. 5(c)]. The fits use Breit-Wigner functions convolved with Gaussians for the signals, where the Breit-Wigner masses and instrumental resolutions are

TABLE III. The branching fractions for $\chi_{cJ} \to \Lambda(1520)\bar{\Lambda}(1520)$. The errors are statistical only, and the upper limit is at the 90% C.L.

Quantity	χ_{c0}	χ_{c1}	χ_{c2}
$N_{\rm obs}$	28.1 ± 9.8	<6.9	28.9 ± 7.4
$\varepsilon(\%)$	17.1 ± 0.1	16.3 ± 0.1	12.2 ± 0.1
$\mathcal{B}(\Lambda(1520) \to pK)(\%)$	22.5	22.5	22.5
$\mathcal{B}(\chi_{cJ} \to \Lambda(1520)\bar{\Lambda}(1520))$ (10^{-4})	3.18 ± 1.11	<0.86	5.05 ± 1.29

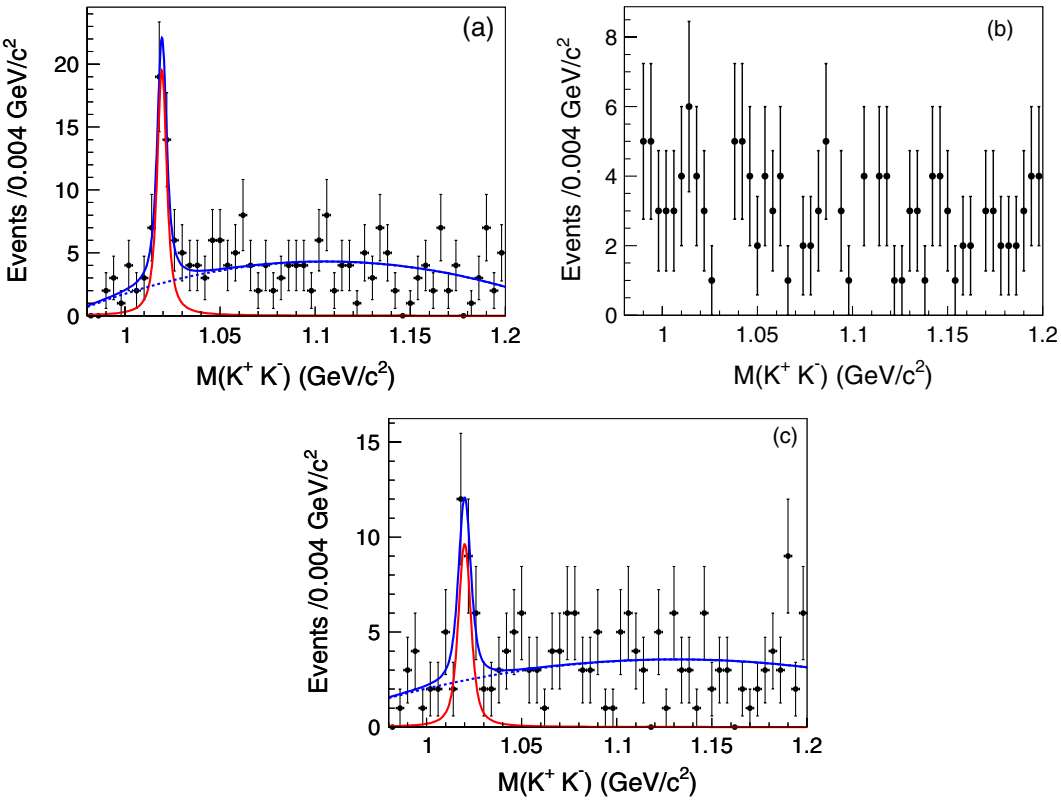

FIG. 5 (color online). K^+K^- invariant mass distributions and fits to the spectra in the decays of (a) χ_{c0} and (c) χ_{c2}. Dots with error bars are data and solid lines represent the fit results. Dashed curves are background shapes. For decays of (b) χ_{c1}, ϕ is not seen clearly and the upper limit at the 90% C.L. is given.

free parameters and resonance widths are fixed at their PDG [1] values, and a Chebyshev polynomial for the background. The observed numbers of events, $N_{\rm obs}$, for $\chi_{cJ} \to p\bar{p}\phi$ are listed in Table IV, as well as an upper limit at the 90% C.L. for $\chi_{c1} \to p\bar{p}\phi$ using a Bayesian method. The branching fractions are estimated as

$$\mathcal{B}(\chi_{cJ} \to p\bar{p}\phi) = \frac{N_{\rm obs}}{N_{\psi'} \cdot \mathcal{B}(\psi' \to \gamma\chi_{cJ}) \cdot \mathcal{B}(\phi \to K^+K^-) \cdot \varepsilon}$$

and the upper limit at the 90% C.L. is calculated as:

$$\mathcal{B}(\chi_{c1} \to p\bar{p}\phi) < \frac{N_{\rm obs}}{N_{\psi'} \cdot \mathcal{B}(\psi' \to \gamma\chi_{c1}) \cdot \mathcal{B}(\phi \to K^+K^-) \cdot \varepsilon \cdot (1-\sigma_{\rm sys})},$$

TABLE IV. The branching fractions for $\chi_{cJ} \to p\bar{p}\phi$. The errors are statistical only, and the upper limit is at the 90% C.L.

Quantity	χ_{c0}	χ_{c1}	χ_{c2}
$N_{\rm obs}$	42.4 ± 8.2	<13.3	24.4 ± 6.8
$\varepsilon(\%)$	13.9 ± 0.1	17.7 ± 0.1	17.7 ± 0.1
$\mathcal{B}(\phi \to K^+K^-)(\%)$	48.9	48.9	48.9
$\mathcal{B}(\chi_{cJ} \to p\bar{p}\phi)$ (10^{-5})	6.12 ± 1.18	<1.58	3.04 ± 0.85

where detection efficiencies are determined from MC simulation as described above. The results are summarized in Table IV.

VI. SYSTEMATIC UNCERTAINTY

The main contributions to the branching fraction systematic uncertainties originate primarily from the tracking,

TABLE V. Systematic uncertainties expressed in percent (%) for the decay modes $\chi_{cJ} \to p\bar{p}K^+K^-$ and $\chi_{cJ} \to \Lambda(1520)\bar{\Lambda}(1520)$.

	$\chi_{cJ} \to p\bar{p}K^+K^-$			$\chi_{cJ} \to \Lambda(1520)\bar{\Lambda}(1520)$		
	χ_{c0}	χ_{c1}	χ_{c2}	χ_{c0}	χ_{c1}	χ_{c2}
Tracking	8.0	8.0	8.0	8.0	8.0	8.0
PID	8.0	8.0	8.0	8.0	8.0	8.0
Photon recon.	1.0	1.0	1.0	1.0	1.0	1.0
Kinematic Fit	1.4	1.6	2.3	1.4	1.6	2.3
Fitting	1.5	0.6	0.0	0.0	0.0	0.0
Mass window	4.2	6.0	2.8	8.2	...	11.0
α value	...	...	...	3.3	...	4.1
Branching fraction	3.2	4.3	4.0	7.0	7.6	7.4
$N_{\psi'}$	4.0	4.0	4.0	4.0	4.0	4.0
Efficiency	5.0	1.2	5.9	...	...	...
Total	14.2	14.3	14.5	16.6	14.3	18.5

TABLE VI. Systematic uncertainties expressed in percent (%) for the decay modes $\chi_{cJ} \to \bar{p}K^+\Lambda(1520) + \text{c.c.}$ and $\chi_{cJ} \to p\bar{p}\phi$.

	$\chi_{cJ} \to \bar{p}K^+\Lambda(1520) + \text{c.c.}$			$\chi_{cJ} \to p\bar{p}\phi$		
	χ_{c0}	χ_{c1}	χ_{c2}	χ_{c0}	χ_{c1}	χ_{c2}
Tracking	8.0	8.0	8.0	8.0	8.0	8.0
PID	8.0	8.0	8.0	8.0	8.0	8.0
Photon recon.	1.0	1.0	1.0	1.0	1.0	1.0
Kinematic Fit	1.4	1.6	2.3	1.4	1.6	2.3
Fitting	9.4	5.9	6.8	4.5	···	4.7
Mass window	2.2	3.6	8.8	2.1	···	1.0
α value	2.8	2.6	2.2	4.0	3.9	2.5
Branching fraction	5.4	6.2	5.9	3.4	4.4	4.1
$N_{\psi'}$	4.0	4.0	4.0	4.0	4.0	4.0
Total	16.6	15.5	17.7	14.1	13.5	14.0

particle identification, photon reconstruction, kinematic fit, branching fractions of the intermediate states (from PDG [1]), total number of ψ' events, fitting procedure, and the event generator. The contributions of each item are summarized in Table V for $\chi_{cJ} \to p\bar{p}K^+K^-$, $\Lambda(1520)\bar{\Lambda}(1520)$ and Table VI for $\bar{p}K^+\Lambda(1520) + \text{c.c.}$ and $p\bar{p}\phi$.

From analyses of very clean $J/\psi \to K^*K$ and $J/\psi \to p\bar{p}\pi^+\pi^-$ decays, the tracking efficiency for MC simulated events is found to agree with that determined using data to within 2% for each charged track. Hence, 8% is taken as the systematic uncertainty for the four charged track final state.

The candidates of the selected final state require tracks be identified as p, $\bar{p}$, K^+, or K^-. Comparing data and MC event samples for $J/\psi \to \pi^+\pi^- p\bar{p}$ and $J/\psi \to K^*K$, a difference in MC and data particle identification efficiency of 2% is obtained for each particle. Hence, 8% is taken as the systematic uncertainty for $p\bar{p}K^+K^-$ identification.

Photon reconstruction efficiency is studied using $\psi' \to \pi^+\pi^- J/\psi \to \gamma\pi^+\pi^- p\bar{p}$, and the difference between data and MC is about 1% per photon [12].

To estimate the uncertainty from kinematic fitting, a $\psi' \to \gamma\chi_{cJ} \to \gamma p\bar{p}\pi^+\pi^-$ sample is selected to study efficiency differences between data and MC. Errors of 1.4%, 1.6%, and 2.3% are obtained for decays of χ_{c0}, χ_{c1}, and χ_{c2}, respectively.

Uncertainties due to the decay model used in simulation for two-body and three-body decay channels are estimated by varying the α values in the decay angular distributions $1 + \alpha\cos^2\theta$. For two-body decay channels, α is varied over a range such that the angular distribution in MC is consistent with that of data. For three-body decays, the accuracy of the angular distributions in data are limited by low statistics. To be conservative, we vary α from -1 to 1 and the resulting differences are taken as the systematic uncertainty.

Uncertainties in the fitting procedure are obtained by altering background shapes and fit intervals. Uncertainties from the mass window requirements, obtained by changing the requirements, of χ_{cJ}, $\Lambda(1520)$, $\bar{\Lambda}(1520)$, and ϕ are shown.

Uncertainties in the reconstruction efficiency for $\chi_{cJ} \to p\bar{p}K^+K^-$ due to other possible intermediate states, $\chi_{c1} \to \bar{p}K^+\Lambda(1600) + \text{c.c.}$ and χ_{c0}, $\chi_{c2} \to \bar{p}K^+\Lambda(1670) + \text{c.c.}$, which are not pronounced in the data, are summarized in Table V. Both masses and widths of $\Lambda(1600)$ and $\Lambda(1670)$ are poorly determined, and their branching fractions are not available. Their branching fractions are taken conservatively as 5×10^{-6}, and the systematic uncertainties are the differences between with and without the intermediate states.

The total number of ψ' events with an uncertainty of 4% is obtained by studying inclusive hadronic ψ' decays [12]. The total systematic uncertainty is obtained by summing up uncertainties contributed from all individual sources in quadrature.

VII. RESULTS AND DISCUSSION

The measured branching fractions for the 12 decay modes decaying to $p\bar{p}K^+K^-$ are summarized in Table VII. From the 106×10^6 ψ' decays observed by BESIII at BEPCII, we report first measurements of these branching fractions with uncertainties ranging from 20% to 40%. With larger statistics in future BESIII running, we expect to improve these measurements and to be able to observe $\Lambda(1520)\bar{\Lambda}(1520)$ in χ_{c1} decays. The excited baryon $\Lambda(1520)\bar{\Lambda}(1520)$ decays provide new information for evaluating model predictions of χ_{cJ} hadronic decays.

TABLE VII. Summary of branching fractions for 12 χ_{cJ} decay modes to $p\bar{p}K^+K^-$. The first errors are statistical, and the second ones are systematic. The upper limits are at the 90% C.L. including the systematic errors.

	χ_{c0}	χ_{c1}	χ_{c2}
$\mathcal{B}(\chi_{cJ} \to p\bar{p}K^+K^-)$ (10^{-4})	$1.24 \pm 0.20 \pm 0.18$	$1.35 \pm 0.15 \pm 0.19$	$2.08 \pm 0.19 \pm 0.30$
$\mathcal{B}(\chi_{cJ} \to \bar{p}K^+\Lambda(1520) + \text{c.c.})$ (10^{-4})	$3.00 \pm 0.58 \pm 0.50$	$1.81 \pm 0.38 \pm 0.28$	$3.06 \pm 0.50 \pm 0.54$
$\mathcal{B}(\chi_{cJ} \to \Lambda(1520)\bar{\Lambda}(1520))$ (10^{-4})	$3.18 \pm 1.11 \pm 0.53$	<1.00	$5.05 \pm 1.29 \pm 0.93$
$\mathcal{B}(\chi_{cJ} \to p\bar{p}\phi)$ (10^{-5})	$6.12 \pm 1.18 \pm 0.86$	<1.82	$3.04 \pm 0.85 \pm 0.43$

ACKNOWLEDGMENTS

The BESIII collaboration thanks the staff of BEPCII and the computing center for their hard efforts. This work is supported in part by the Ministry of Science and Technology of China under Contract No. 2009CB825200; National Natural Science Foundation of China (NSFC) under Contracts No. 10625524, No. 10821063, 10825524, 10835001, No. 10875113, No. 10935007, No. 10979038, No. 11005109, No. 11079030; the Chinese Academy of Sciences (CAS) Large-Scale Scientific Facility Program; CAS under Contracts No. KJCX2-YW-N29, No. KJCX2-YW-N45; 100 Talents Program of CAS; Research Fund for the Doctoral Program of Higher Education of China under Contract No. 20093402120022; Istituto Nazionale di Fisica Nucleare, Italy; Siberian Branch of Russian Academy of Science, joint project No. 32 with CAS; U.S. Department of Energy under Contracts No. DE-FG02-04ER41291, No. DE-FG02-91ER40682, No. DE-FG02-94ER40823; University of Groningen (RuG) and the Helmholtzzentrum fuer Schwerionenforschung GmbH (GSI), Darmstadt; WCU Program of National Research Foundation of Korea under Contract No. R32-2008-000-10155-0.

[1] K. Nakamura *et al.* (Particle Data Group), J. Phys. G **37**, 075021 (2010).
[2] J. Bolz, P. Kroll, and G. A. Schuler, Phys. Lett. B **392**, 198 (1997).
[3] S. M. Wong, Eur. Phys. J. C **14**, 643 (2000).
[4] S. M. Wong, Nucl. Phys. **A674**, 185 (2000).
[5] E. Braaten and J. Lee, Phys. Rev. D **67**, 054007 (2003).
[6] J. Z. Bai *et al.* (BES Collaboration), Phys. Rev. D **67**, 112001 (2003).
[7] M. Ablikim *et al.* (BESIII Collaboration), Nucl. Instrum. Methods Phys. Res., Sect. A **614**, 345 (2010).
[8] S. Jadach, B. F. L. Ward, and Z. Was, Comput. Phys. Commun. **130**, 260 (2000).
[9] S. Jadach, B. F. L. Ward, and Z. Was, Phys. Rev. D **63**, 113009 (2001).
[10] R. G. Ping *et al.*, Mod. Phys. Lett. A **24**, 23 (2009).
[11] R. G. Ping, Chinese Phys. C **32**, 599 (2008).
[12] M. Ablikim *et al.* (BESIII Collaboration), Phys. Rev. D **81**, 052005 (2010).